Cellular and Molecular Life Sciences (2023) 80:154
https://doi.org/10.1007/s00018-023-04803-x

ORIGINAL ARTICLE

Tetraspanin Tspan8 restrains interferon signaling to stabilize intestinal epithelium by directing endocytosis of interferon receptor

Jiang Min[1] · Shenglan Yang[1] · Yang Cai[1] · David R. Vanderwall[2] · Zhiping Wu[2] · Shuping Li[1] · Songlan Liu[1] · Beibei Liu[1] · Jie Wang[1] · Yingjun Ding[1] · Junxiong Chen[1] · Chao Jiang[1] · Jonathan D. Wren[3] · Anna Csiszar[1] · Zoltan Ungvari[1] · Céline Greco[4] · Tomoharu Kanie[1] · Junmin Peng[2] · Xin A. Zhang[1]

Received: 15 December 2022 / Revised: 25 April 2023 / Accepted: 8 May 2023 / Published online: 19 May 2023

Abstract

Inflammation can impair intestinal barrier, while increased epithelial permeability can lead to inflammation. In this study, we found that the expression of Tspan8, a tetraspanin expressed specifically in epithelial cells, is downregulated in mouse model of ulcerative disease (UC) but correlated with those of cell–cell junction components, such as claudins and E-cadherin, suggesting that Tspan8 supports intestinal epithelial barrier. Tspan8 removal increases intestinal epithelial permeability and upregulates IFN-γ-Stat1 signaling. We also demonstrated that Tspan8 coalesces with lipid rafts and facilitates IFNγ-R1 localization at or near lipid rafts. As IFN-γ induces its receptor undergoing clathrin- or lipid raft-dependent endocytosis and IFN-γR endocytosis plays an important role in Jak-Stat1 signaling, our analysis on IFN-γR endocytosis revealed that Tspan8 silencing impairs lipid raft-mediated but promotes clathrin-mediated endocytosis of IFN-γR1, leading to increased Stat1 signaling. These changes in IFN-γR1 endocytosis upon Tspan8 silencing correlates with fewer lipid raft component GM1 at the cell surface and more clathrin heavy chain in the cells. Our findings indicate that Tspan8 determines the IFN-γR1 endocytosis route, to restrain Stat1 signaling, stabilize intestine epithelium, and subsequently prevent intestine from inflammation. Our finding also implies that Tspan8 is needed for proper endocytosis through lipid rafts.

Keywords Caveolin · Clathrin · Epithelial permeability · Lipid raft · Stat1 · Vesicular trafficking

Introduction

Intestinal epithelium provides a selectively permeable barrier to support whole body homeostasis. The epithelial barrier permits absorption of water and nutrients, while it also limits influx of noxious substances, such as microorganisms and their products, into intestine wall and then systemic circulation [1, 2]. The intestinal barrier is maintained mainly by cell–cell junctions, such as tight junction (TJ) and adherens junction (AJ). The components of TJs include transmembrane proteins occludins, claudins, and junctional adhesion molecule and cytoplasmic proteins ZO-1, ZO-2, and ZO-3, while those of AJs include transmembrane protein E-cadherin and cytoplasmic proteins catenins [3, 4].

Intestinal epithelial hyper-permeability due to compromised epithelial barrier, which is presented as damaged cell–cell junctions, is briefly observed in the inflammatory conditions of mouse colitis models and patients with inflammatory bowel disease (IBD) [5]. For example, alterations in distribution and formation of TJ and AJ exist during inflammation [6–8]. Paracellular hyper-permeability of intestine epithelium in turn enhances the exposure of luminal antigens to abluminal immune cells, to initiate inflammatory cascade and further compromise epithelial barrier [9]. Thus, mucosal inflammation of intestine is the main factor influencing epithelial stability.

Shenglan Yang and Yang Cai contributed equally.

✉ Xin A. Zhang
xin-zhang-1@ouhsc.edu

1 University of Oklahoma Health Sciences Center, Oklahoma City, USA

2 Departments of Structural Biology and Developmental Neurobiology, St. Jude Children's Research Hospital, Memphis, TN 38105, USA

3 Oklahoma Medical Research Foundation, Oklahoma City, USA

4 Department of Pain and Palliative Care Unit, Hôpital Necker-Enfants Malades, AP-HP, Paris, France

As a tetraspanin [10, 11], Tspan8 promote the proliferation, migration, invasion, and metastasis of cancer cells from multiple tissue sources, including glioma, melanoma, hepatocarcinoma, and ovarian, gastric, and colorectal cancers [12–17]. Tspan8 also regulates the stemness of breast and pancreatic cancers [18, 19]. Therefore, Tspan8 is considered as a promising therapeutic target against cancer [20–22]. However, the in-depth mechanisms for Tspan8 to enhance malignancy are still incomplete, and other pathophysiological functions that Tspan8 regulates remain largely unknown.

As shown in this study, Tspan8 silencing attenuates intestinal epithelial barrier function, which results from the increase of IFN-γ-Stat1 signaling. Switch of IFN-γ receptor (IFN-γR1) endocytosis from lipid raft-dependent route to clathrin-dependent route and subsequent more activation of Stat1 signaling cause this increase, in Tspan8-silenced cells. Tspan8 confines IFN-γR1 at or near lipid raft and promotes lipid raft-mediated endocytosis of IFN-γR1 for its turnover, to prevent hyper-activation of IFN-γ-Stat1 signaling, breakdown of epithelial barrier, and then inflammation of intestine.

Materials and methods

Reagents and cells

Information about all antibodies is attached in Table S1. Information about the reagents is attached in supplemental Table S2. HT29, Caco-2, and SW480 colorectal cancer cell lines were purchased from ATCC. All cells were cultured in Dulbecco's Modified Eagle Medium (DMEM; Corning) with 10% FBS (Biowest, TX) for HT29 and SW480 cells and 20% FBS for Caco-2 cells, 100 units/ml penicillin, and 100 units/ml streptomycin.

Cell preparation

HT29 cells were infected by scramble or Tspan8 shRNA virus particles. After 48 h, cells were treated with 1 μg/ml puromycin for 1 week. Then, the puromycin-resistant cells were sorted by flow cytometry to enrich the Tspan8 knocked-down population, which we termed HT29-KD cells. The scramble group was sorted by flow cytometry and we obtained population that we called HT29-NS cells. Virus particles were prepared and cells were infected by following the previously described protocol [23]. The plasmids TRIP3-EF1α and TRIP3-EF1α-Tspan8 (kindly granted by Drs. Claude Boucheix and Anne Dubart-Kupperschmitt) were separately transfected into SW480 cells [16, 24]. Tspan8-positive cells were sorted by flow cytometry and termed SW480-Tspan8 cells. The control group named SW480-con cells. Caco-2 cells were transfected with Tspan8 and control siRNA (Ambion) via Lipofectamine3000 (ThermoFisher) and used for the experiments at 48 h post-transfection.

Clonogenic assay

Harvesting a single cell suspension was performed by the treatment of 0.05% trypsin. Three hundred cells were cultured in 2 ml of DMEM complete medium in one well of 6-well plate. Every kind of cell had duplicates. After 2 weeks, the media were removed, the cells were fixed with 2 ml of cold methanol for 5 min, and the clones were stained with 0.5% crystal violet for 15 min and rinsed with water five times. The plates were dried at room temperature (RT), numbers of the clones were counted, and plating efficiency is the ratio of the number of colonies to the number of cells seeded [25] and is used for the readout of the assay.

Trans-epithelial electrical resistance (TEER) and fluorescent dextran diffusion analyses

Cell culture wells were coated by Collagen-I (0.8 mg/ml), HT29 cells were grown in conditional DMEM medium, in which glucose was replaced by galactose (5 mM) and each nonessential amino acid was added to a final concentration of 0.1 mM. The cells were confluent for 5 days and developed the differentiated monolayer [26, 27].

TEER was analyzed with electric cell-substrate impedance sensing (ECIS) system. All wells in a 96W1E+ plate were coated according to the above mentioned protocol. A cell suspension (2×10^5 cells in 200 μl of conditioned media) was loaded into each well of a 96W1E+ plate. Each group of cells had 12 replicated wells per experiment. After 48 h, the media were changed on a daily basis. The prepared plates were tested by the ECIS system according to the manufacturer's protocol. The 96W1E+ plate, ECIS system, and analysis software were purchased from Applied Biophysics, New York.

For FITC-dextran diffusion experiments, cell culture inserts (0.4 μm) in 24-well plates were coated with Collagen-I (0.8 mg/ml), and 2×10^5 cells in 200 μl of conditional medium were added into each insert. Each cell group had triplicates in each experiment. After 5-day culture, the media in the inserts or upper chamber were replaced with the condition media containing either 4 kDa or 40 kDa FITC-dextran (4 mg/ml), while the media in lower chamber remained intact. After incubation at 37 °C for 30 min for HT29 monolayers and for various periods of time for Caco-2 monolayers, the conditioned media in the lower chamber were collected and measured with a Perkin Elmer EnVision® Multilabel Reader [28].

Flow cytometry

Cells at 80–90% confluence were detached with 0.1% Trypsin. For the protein test in cell surface, cells were incubated with primary antibody (Ab) for 1 h on ice. Then, cells were washed three times with ice-cold PBS and incubated with fluorescence conjugated secondary Ab for 1 h on ice. After cells were washed three more times, we analyzed the cells with the Stratedigm S1400Exi flow cytometry platform. For the protein test in total level, cells were fixed in 4% paraformaldehyde and then permeabilized with 0.1% Brij98 for 45 s. Following the method mentioned above, cells were then stained sequentially with primary and secondary Ab, and analyzed with the Stratedigm S1400Exi flow cytometry platform.

Western blot

Cells at 80–90% confluence were washed three times with ice-cold PBS, and then scraped and lysed for 30 min on ice with RIPA lysis buffer (1% Triton, 0.2% SDS, 50 mM Tris–HCl at pH 7.4, 150 mM NaCl and 2 mM EDTA) supplemented with protease inhibitors (1 mM PMSF, 10 µg/ml aprotinin and 10 µg/ml leupeptin). Then, cells were centrifuged at 13,000*g* at 4 °C for 20 min. The supernatants were collected, mixed with 2 × Laemmli sample buffer, and boiled at 98 °C for 3 min. The protein samples were subjected to SDS-PAGE before transfer to a nitrocellulose membrane. The membrane was blocked with 5% low fat milk in PBS/0.05% Tween-20, blotted sequentially with primary Ab at 4 °C overnight and HRP-conjugated secondary Ab at RT for 2 h, and washed five times for chemiluminescence analysis.

Proximity ligation assay

Cells grown on glass coverslips were fixed with 4% paraformaldehyde at RT for 10 min, permeabilized with 0.1% Triton X-100 at RT for 40 s, blocked with 15% goat serum at RT for 1 h, and incubated with primary antibodies at 4 °C overnight. The Duolink® PLA Fluorescence protocol was followed for the subsequent steps of PLA with Duolink® PLA reagents kit (Sigma). The cells were then counterstained with DAPI for nucleus, mounted, and observed with a Leica SP8 confocal microscope.

Immunofluorescence and confocal microscopy

Cells were cultured on glass coverslips for 2 days, washed with PBS, and fixed with 4% paraformaldehyde, followed by cell membrane permeabilization with 0.1% Brij 98 and blockade with 10% goat serum. The cells were incubated sequentially with primary Abs, fluorescence-conjugated secondary Abs, and DAPI. Then, the cells were washed, mounted, and imaged with a Leica SP8 confocal microscope.

Structured illumination microscopy (SIM) and image analysis

Cells cultured on the Nunc Lab-Tek II chambered coverglass were fixed with 4% paraformaldehyde at room temperature for 10 min, permeabilized, washed with PBS, and blocked with 15% goat serum in PBS at room temperature for 45 min. Then, the cells were incubated with primary Abs at 4 °C overnight and fluorochrome-conjugated cholera toxin B subunit (CTxB) or secondary Abs at room temperature for 1 h and DAPI for 10 min. After each incubation, the cells were washed 3 times with PBS. The cells were observed and imaged with a Nikon N-SIM-E/STORM super-resolution microscope equipped with a 100 ×/1.49 NA CFI SR HP Apo TIRF 100XC Oil objective lens (MRD01995, Nikon), LU-N3 compact laser unit (248071, Nikon), and ORCA-Flash4.0 V3 Digital CMOS camera (C13440, HAMAMATSU). Image stacks of appropriate z-steps were taken in 0.1 µm increments to ensure Nyquist sampling. The images were then computationally reconstructed for 3D rendering and subjected to image registration using Nikon NIS-Elements software.

Proteomic analysis by tandem mass tag (TMT) strategy and mass spectrometry (MS)

Proteomic analysis was performed using a previously optimized protocol [29, 30]. The Four HT29 cell pellets (2 Mock, 2 TSPAN8 KD, ~ 8 million cells) were lysed in 500 µl of lysis buffer (50 mM HEPES, pH 8.5, 8 M urea, and 0.5% sodium deoxycholate). Protein concentration of the lysate was calculated with a commercial BCA kit (Thermo Scientific), followed by proteolysis with LysC (peptide:enzyme = 1:100 w/w) for 2 h at 21 °C. To optimize trypsin digestion, urea was diluted to 2 M with 50 mM HEPES, followed by overnight trypsinization at 21 °C. Cys residues were reduced and alkylated by iodoacetamide. Digested peptides were desalted on C18 Ultra-Micro Spin Columns (Harvard Apparatus), resuspended in 50 mM HEPES pH 8.5 to ~ 1 µg/µl, labeled with TMT reagents (peptide:TMTpro reagent = 1:1.5 w/w), and pooled at 1:1:1:1 peptide ratio.

The pooled TMT-labeled peptides were dried and resuspended in 5% formic acid for analysis by two dimensional liquid chromatography (LC) and MS [31]. First, the sample was fractionated into 40 concatenated fractions

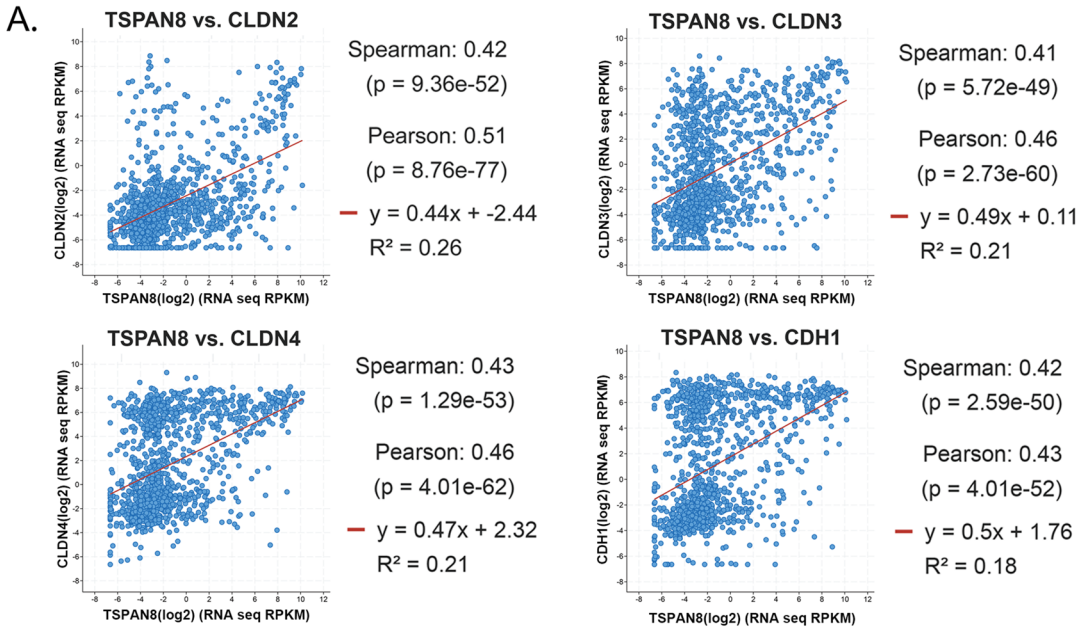
A.
TSPAN8 vs. CLDN2
CLDN2(log2) (RNA seq RPKM)
TSPAN8(log2) (RNA seq RPKM)
Spearman: 0.42
(p = 9.36e-52)
Pearson: 0.51
(p = 8.76e-77)
y = 0.44x + -2.44
R² = 0.26
TSPAN8 vs. CLDN3
CLDN3(log2) (RNA seq RPKM)
TSPAN8(log2) (RNA seq RPKM)
Spearman: 0.41
(p = 5.72e-49)
Pearson: 0.46
(p = 2.73e-60)
y = 0.49x + 0.11
R² = 0.21
TSPAN8 vs. CLDN4
CLDN4(log2) (RNA seq RPKM)
TSPAN8(log2) (RNA seq RPKM)
Spearman: 0.43
(p = 1.29e-53)
Pearson: 0.46
(p = 4.01e-62)
y = 0.47x + 2.32
R² = 0.21
TSPAN8 vs. CDH1
CDH1(log2) (RNA seq RPKM)
TSPAN8(log2) (RNA seq RPKM)
Spearman: 0.42
(p = 2.59e-50)
Pearson: 0.43
(p = 4.01e-52)
y = 0.5x + 1.76
R² = 0.18

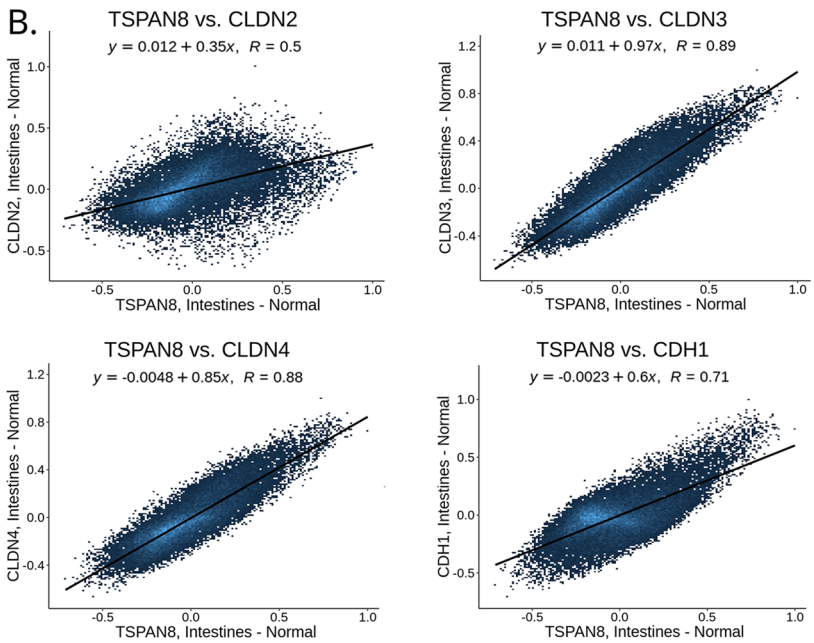
B.
TSPAN8 vs. CLDN2
y = 0.012 + 0.35x, R = 0.5
CLDN2, Intestines - Normal
TSPAN8, Intestines - Normal
TSPAN8 vs. CLDN3
y = 0.011 + 0.97x, R = 0.89
CLDN3, Intestines - Normal
TSPAN8, Intestines - Normal
TSPAN8 vs. CLDN4
y = -0.0048 + 0.85x, R = 0.88
CLDN4, Intestines - Normal
TSPAN8, Intestines - Normal
TSPAN8 vs. CDH1
y = -0.0023 + 0.6x, R = 0.71
CDH1, Intestines - Normal
TSPAN8, Intestines - Normal

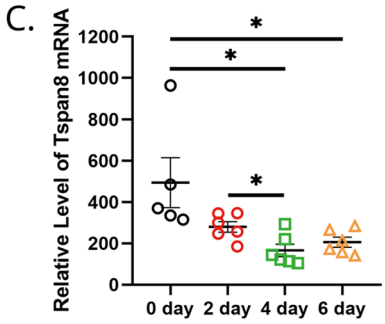
C.
Relative Level of Tspan8 mRNA
0 day
2 day
4 day
6 day

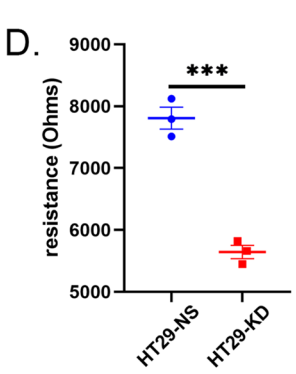
D.
resistance (Ohms)
HT29-NS
HT29-KD

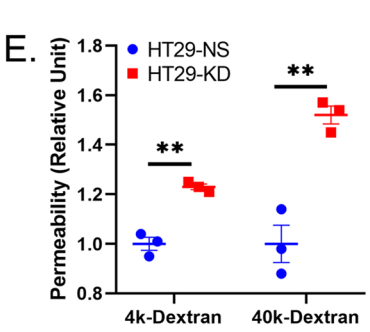
E.
HT29-NS
HT29-KD
Permeability (Relative Unit)
4k-Dextran
40k-Dextran

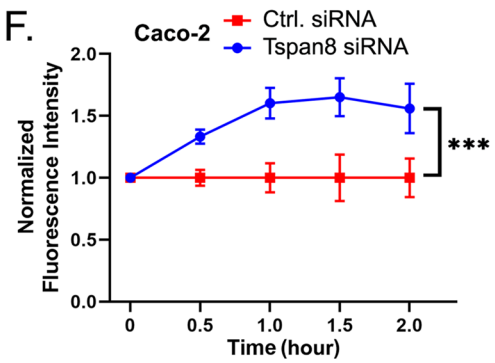
F.
Caco-2
Ctrl. siRNA
Tspan8 siRNA
Normalized Fluorescence Intensity
Time (hour)

◂**Fig. 1** Tspan8 plays a role in regulating intestinal epithelial permeability. **A** Gene expression correlation analysis was performed with the cBioPortal search and analysis tool, to examine the relationships between Tspan8 and CLDN2, CLDN3, CLDN4, or CDH1 at the mRNA level cross 1156 cancer cell lines. **B** Gene expression correlation analysis was performed with the Correlation AnalyzeR search and analysis tool and presented as scatter plot, to assess the genome-wide co-expression links between TSPAN8 and CLDN2, CLDN3, CLDN4, or CDH1 in normal intestine tissue. R value is determined by Pearson correlation coefficient. **C** Dot plot of Tspan8 expression levels in mouse with DSS feeding from NCBI's Gene Expression Omnibus database (GDS3859). **D** In the ECIS barrier function assay, trans-epithelium electricity resistance (TEER) was measured in 144 h (mean ± SEM, $n = 3$ individual experiments). ***$p < 0.001$. **E**, **F** In vitro barrier functions of HT29 (**E**) and Caco-2 (**F**) monolayers were examined with the abilities of 4 kDa and/or 40 kDa FITC-dextran to pass through the monolayers (mean ± SEM, $n = 3$ individual experiments). **$p < 0.01$ and ***$p < 0.001$

by offline basic pH reverse phase HPLC. Each fraction was analyzed by acidic pH LC–MS/MS on a CoAnn 75 µm × 20 cm column online with a Q Exactive HF Orbitrap (Thermo Fisher). Peptides were eluted by a ~ 90 min gradient (buffer A: 0.2% formic acid, 3% DMSO; buffer B: 0.2% formic acid, 3% DMSO, 67% acetonitrile). MS settings included the MS1 scan (~ 450–1600 *m/z*, 60,000 resolution, 1×10^6 AGC and 50 ms maximal ion time) and 20 data-dependent MS2 scans (fixed first mass of 120 *m/z*, 60,000 resolution, 1×10^5 AGC, ~ 110 ms maximal ion time, HCD, ~ 32% normalized collision energy, ~ 1.0 *m/z* isolation window with 0.25 *m/z* offset, and ~ 10 s dynamic exclusion) [32].

Data analysis was performed by the JUMP software suite [33]. The JUMP search algorithm integrates spectrum pattern matching and de novo sequencing for improved sensitivity and specificity. MS raw files were converted into mzXML format and searched against a human Uniprot target-decoy database for estimation of the False Discovery Rate (FDR) [34]. Search parameters were modified, such that precursor and product ion mass tolerance were limited to 10 ppm, along with full tryptic restriction, two missed cleavages, dynamic Met oxidation (+ 15.99491), static TMTpro modification (+ 304.20715), and static Cys carbamidomethylation (+ 57.02146). The matched proteins were filtered to reduce protein FDR under 1%. For quantification, TMT reporter ion intensities for each PSM were extracted and summarized into protein intensities [35]. The comparison between samples was based on moderated *t* test in the limma R package to derive *p* values, which were then derived to FDR values by the Benjamini–Hochberg procedure to correct for multiple hypotheses. Finally, differentially expressed proteins were analyzed by JUMPn to identify significantly perturbed pathways with topological overlap matrices of the protein interaction network [36].

Statistics

All experiments were repeated at least three times. Data are presented as Standard Error of the Mean (SEM). Unpaired *t* test was used to determine the significance of differences. *, **, and *** represent $p < 0.05$, $p < 0.01$, and $p < 0.001$, respectively.

Results

Loss of Tspan8 gives rise to elevated intestine epithelial permeability

To determine the pathophysiological functions of Tspan8, we analyzed the expression profile of Tspan8 in human tissues with Protein Atlas database [37]. Tspan8 is specifically expressed in polarized epithelial cells, especially high in simple column epithelial cells of gastrointestinal tract (Table S3). Analysis on 1156 solid tumor cell lines, most of which are carcinoma cell lines, through cBioportal for Cancer Genomics showed that Tspan8 is positively correlated in gene expression with some claudins and E-cadherin, which are the building blocks of epithelial cell–cell junctions (Fig. 1A; Table S4). Positive correlations in gene expression between Tspan8 and claudin-2, claudin-3, claudin-4, or E-cadherin, also exist in both normal and cancerous intestine tissues, analyzed through the Correlation AnalyzeR [38] (Fig. 1B, Table S5). These results suggest that Tspan8 regulates epithelial cell–cell adhesion or epithelial barrier function.

Compromised epithelial barrier leads to hyper-permeability of intestine epithelia, which is a characteristic of IBD. Interestingly, by examining Tspan8 mRNA expression in mouse colon from DSS-induced ulcerative colitis (UC) model, based on NCBI's Gene Expression Omnibus database (GDS3859), we found that Tspan8 level was gradually downregulated during DSS treatment, compared with the samples without DSS treatment, suggesting that Tspan8 is related to intestine inflammation (Fig. 1C).

To unveil intestine-related functions of Tspan8, we chose HT29 cells, a well-differentiated and polarized colon cancer cell line able to form an epithelium-like monolayer, as an experimental model [26] and had established stable transfectants of Tspan8 knockdown (HT29-KD) and Mock knockdown (HT29-NS) [23] (Fig. S1A). Gene expression profiling analysis on these transfectants showed that *CLDN2* was notably decreased in HT29-KD cells, compared to HT29-NS cells (Fig. S1B), consistent with the conclusion from the bioinformatics correlation analysis described above. These observations prompted us to examine Tspan8 role in epithelial barrier function.

Monolayers of the HT29-NS and HT29-KD cells that had undergone differentiation in a no-glucose medium were measured for trans-epithelium electricity resistance (TEER) with ECIS system. In about 120 h, the TEER of HT29-KD monolayer reached plateau in a much slower pace (Fig. S1C), and the maximal TEER also decreased by about 30% in HT29-KD group, compared with HT29-NS group (Fig. 1D). In addition, we measured the ability of FITC-dextran to pass through the epithelial barrier formed by HT29-NS and HT29-KD cells in vitro. The diffusion of 4 kDa FITC-dextran through HT29-KD monolayer was 20% more than that through HT29-NS monolayer, while the difference in the 40 kDa FITC-dextran diffusion between the two groups went up to 50% (Fig. 1E). To substantiate these observations, we included another widely used experimental model of intestine epithelial permeability, i.e., Caco-2 cells. Silencing Tspan8 in Caco-2 cells via siRNA (Fig. S1D) also markedly increased the diffusion of 4 kDa FITC-dextran through the Caco-2 monolayers (Fig. 1F). Together, these findings suggest that Tspan8 is required for maintaining proper intestinal epithelial barrier function and confines epithelial para-cellular permeability.

Meanwhile, we also examined the effect of Tspan8 silencing on cell survival and apoptosis. In clonogenic assay, the two groups were comparable in anchorage-independent cell survival and proliferation (Fig. S1E); and apoptosis-related proteins of Bax and cleaved caspase-3 were not detectable by Western blot (Fig. S1F), suggesting Tspan8 knockdown does not induce apoptosis or affect cell survival.

Tspan8 inhibits IFN-γ-Stat1 signaling

Increased epithelial permeability is often observed in inflammatory conditions, and whether Tspan8 directly regulates inflammation is unknown. A mass spectrometry (MS) workflow was performed by TMT-based shotgun proteomics [29] on HT29-NS and HT29-KD cells. A total of 43,002 unique peptides were identified and mapped to 7,323 unique proteins using the JUMP suite [33]. Differential expression analysis of the proteomic readout identified 273 proteins whose difference in expression between HT29-NS and HT29-KD passed the FDR-corrected (Benjamini–Hochberg) p value threshold of $p < 0.05$.

Protein–protein interaction and enrichment pathway analyses were performed on these differentially expressed proteins using the JUMPn software [36]. Based on four commonly used pathway databases, i.e., Gene Ontology (GO), KEGG, Hallmark, and Reactome, interferon-induced Stat1 signaling pathways were significantly enriched in HT29-KD cells (Fig. 2A, B and Fig. S2). This finding was recapitulated by gene expression profiling analysis on HT29-NS and HT29-KD cells (Fig. 2A, B and Fig. S2).

Indeed, the levels of total Stat1, p-Stat1 (Tyr^{701}), and p-Stat1 (Ser^{727}) all increased in HT29-KD cells, shown by Western blot, while the level of p-Stat3 (Tyr^{705}) was too low to be detected and total Stat3 was slightly downregulated (Fig. 2C). Nuclear translocation of Stat1 reports its activation. Level of p-Stat1 (Tyr^{701}), which is mainly located inside nucleus, became obviously increased inside nucleus upon Tspan8 knockdown, while total Stat1 proteins were increased in both cytoplasm and nucleus (Fig. 2D). Consistently, immunofluorescence also revealed an obvious increase of nuclear p-Stat1 (Tyr^{701}) in HT29-KD cells (Fig. 2E). Hence, Tspan8 restrains Stat1 activation and signaling.

Mainly interferons (IFNs), and also some interleukins (ILs) including IL-2, IL-6, and IL12 [39–42], activate Stat1 signaling, while Stat3 is a hub of ILs signaling. Hence, Stat1 activation is more specifically attributed to IFNs [43, 44]. To determine whether cytokines enhance Stat1 signaling in HT29-KD cells, we analyzed IFNs, their receptors, and transcriptional targets in microarray. There was no difference in IFNs and their receptors at mRNA level, while mRNA levels of interferon-induced transmembrane-1 (IFITM1), IFITM2, and IFITM3, the specific transcriptional products of the IFNs-induced Stat1 signaling, were substantially elevated in HT29-KD cells (Fig. 3A). At the protein level, IFITM1 and IFITM3 also increased (Fig. 3B). In addition, we also analyzed IFITMs in aforementioned GDS3859 data set, and found that both IFITM1 and IFITM3 were increased steadily during DSS treatment, and Tspan8 was negatively correlated to IFITM3 (Fig. S3). The result indicated that enhanced Stat1 signaling in HT29-KD cells was caused by IFNs.

Then, we measured the main ILs and IFNs in the conditioned media of HT29-NS and HT29-KD cells. Only IL-2 and IFN-γ were detectable but remained comparable between the two groups (Fig. 3C). Because Jak1/2 mediates IFN-induced Stat1 activation, Jak1/2 kinase inhibitor ruxolitinib not only abolished high Stat1 signaling in HT29-KD cells but also completely inhibited the basal level of p-Stat1 (Tyr^{701}) in HT29-NS cells (Fig. 3D). Furthermore, treatment of the cells with exogenous IFN-γ enhanced Stat1 signaling more pronounced in HT29-KD cells than in HT29-NS cells (Fig. 3E). Hence, Stat1 over-activation in HT29-KD is closely related to IFN-γ.

In addition, using SW480 colon cancer cell line, which has almost no endogenous Tspan8 expression, we established SW480 stable transfectant of Tspan8 overexpression (Fig. 3F). The basal level of pY701-Stat1 was not detected in SW480-con and SW480-Tspan8 transfectant cells. IFN-γ induced less increase of p-Stat1 (Tyr^{701}) in SW480-Tspan8 cells than in SW480-con cells at various timepoints, indicating that Tspan8 prohibits IFN-γ-stimulated Stat1 activation (Fig. 3F). Taken together, these results underline that Tspan8 restrains IFN-γ-induced Stat1 signaling.

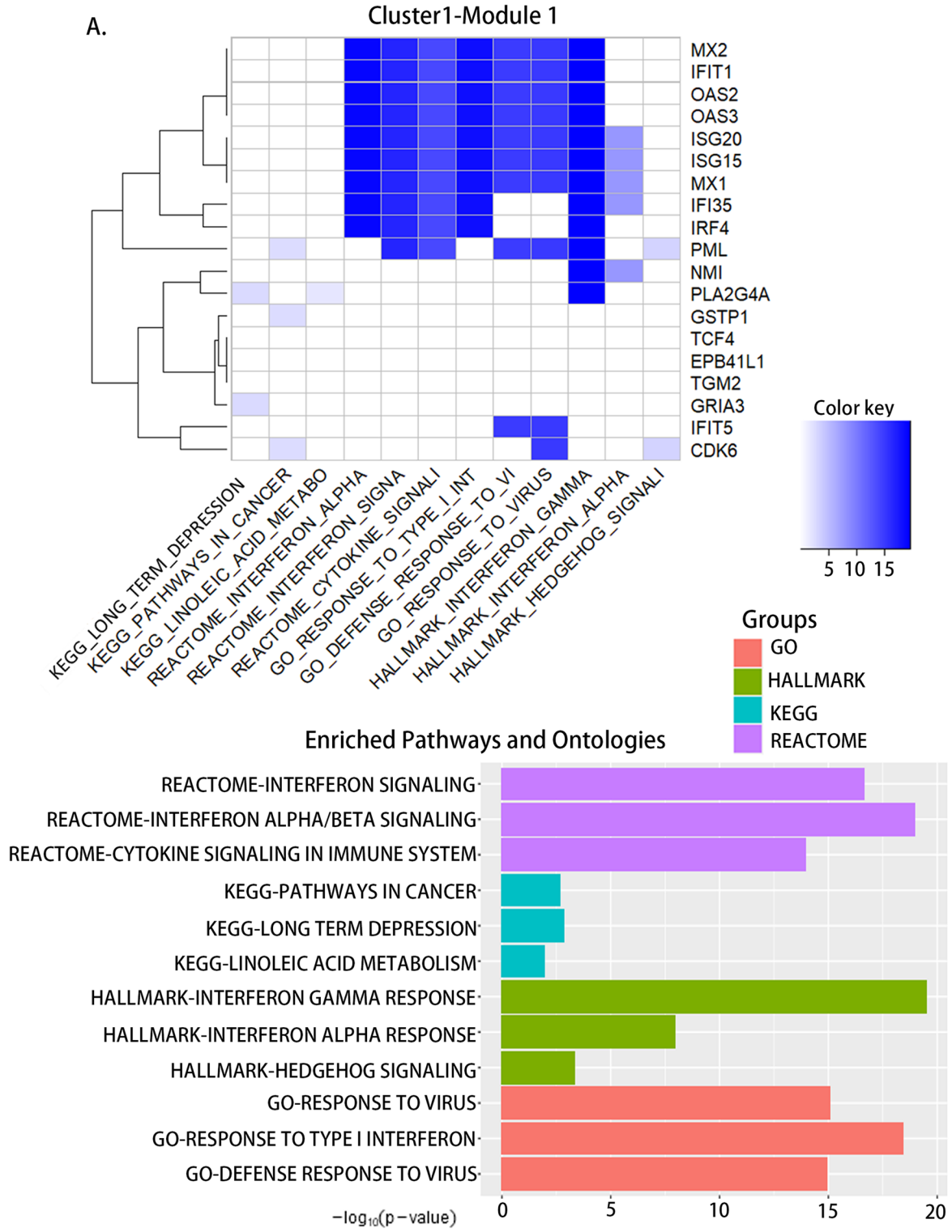

Fig. 2 Tspan8 silencing enhances stat1, not stat3, signaling in colorectal cancer cells. **A**, **B** Altered expression, co-expression, enriched pathway, and JUMPn (see "Methods") analyses on the clusters of differential expression in HT29-KD cells, compared to HT29-NS cells, through the proteomic analysis of tandem mass tag (TMT) strategy and mass spectrometry (MS) in two different modules of upregulated cluster. **C** Stat1, Stat3, and their phosphorylation statuses were analyzed using Western blot. **D** p-Stat1 (Tyr^{701}) and total stat1 in the cytoplasm and nucleus were blotted in HT29-NS and HT29-KD cells. **E** Differential expression and distribution of p-Stat1 (Tyr^{701}) and Tspan8 in HT29-NS and HT29-KD cells are shown in immunofluorescence; p-Stat1 (Tyr^{701}) (AlexaFluor-594, red), Tspan8 (Alex Fluor-488, green), and DAPI (blue)

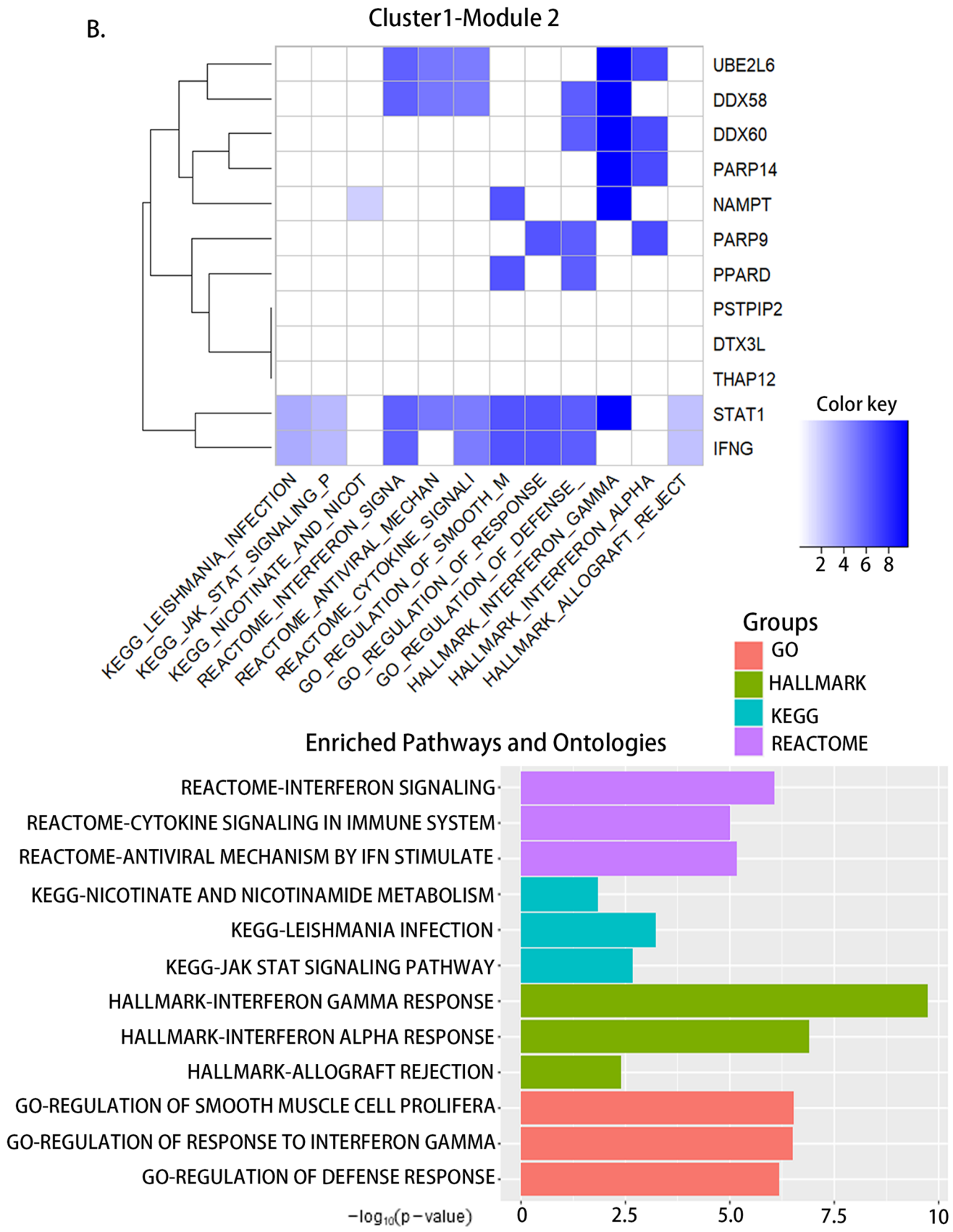

Fig. 2 (continued)

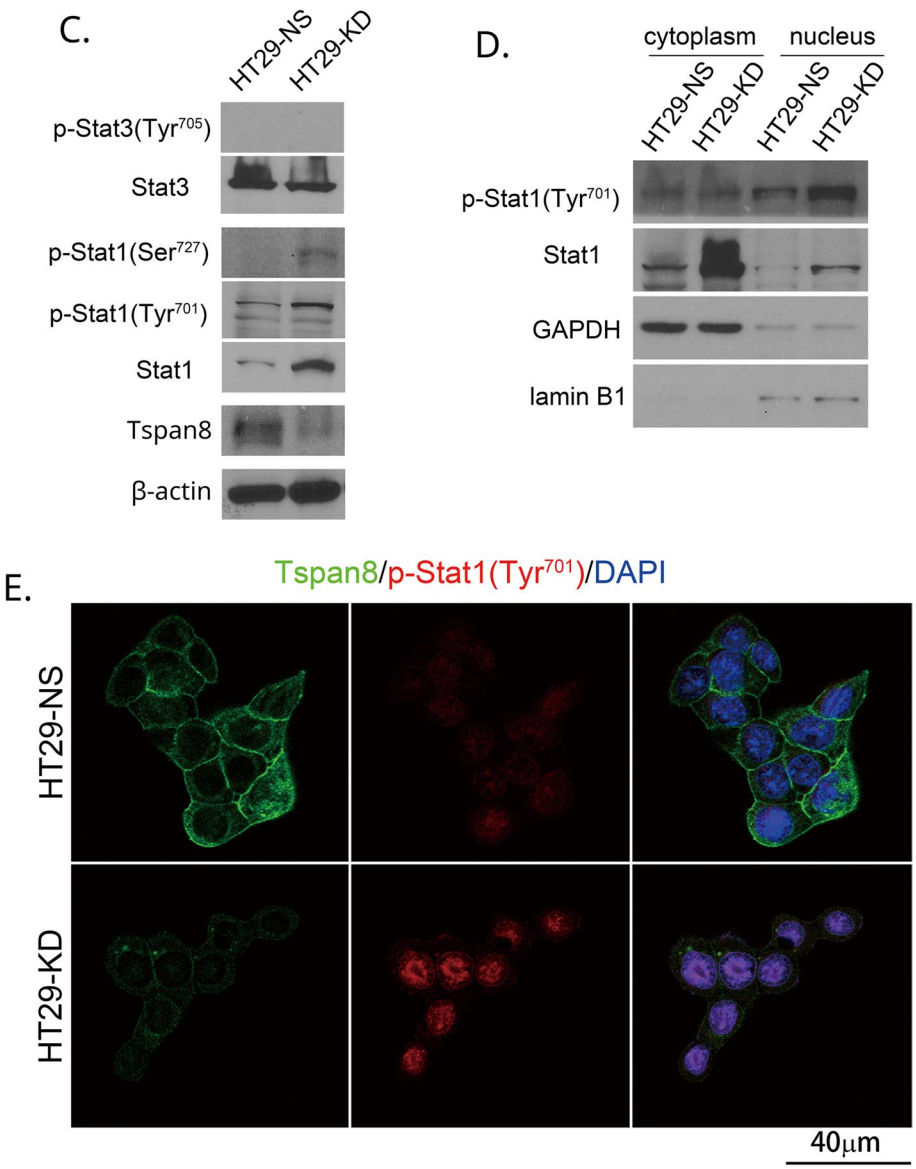

Fig. 2 (continued)

Tspan8 restrains IFN-γ receptor endocytosis and then Stat1 activation

IFNs binding to its receptors typically initiates Jak1–Stat1 signaling cascade, and the ligand–receptor undergoes endocytosis together. The endocytosis is a key process for further and continued activation of Stat1 signaling [45–47]. Flow cytometry showed that, at the surface of HT29-KD cells, IFN-γR1 was notably decreased but IFN-γR2 exhibited no change (Fig. 4A). Western blot revealed that, in total cell lysates, IFN-γR1 increased significantly but again IFN-γR2 remained unchanged (Fig. 4B). Furthermore, IFN-α/β receptors were comparable in two groups (Fig. S4). The results suggest that Tspan8 silencing promotes endocytosis of IFN-γR1 and results in (i) IFN-γR1 accumulation and (ii) more and/or longer Stat1 activation. Furthermore, IFN-γR1 on the cell surface of SW480 transfectants was equivalent between the two groups. When treated with IFN-γ, IFN-γR1 was notably decreased on SW480-con cells but almost remained no change on SW480-Tspan8 cells, compared with those without IFN-γ treatment (Fig. 4C). Tspan8 prohibited IFN-γ-induced endocytosis of IFN-γR1. Hence, Tspan8 restrains IFN-γR1 internalization and subsequently Stat1 signaling.

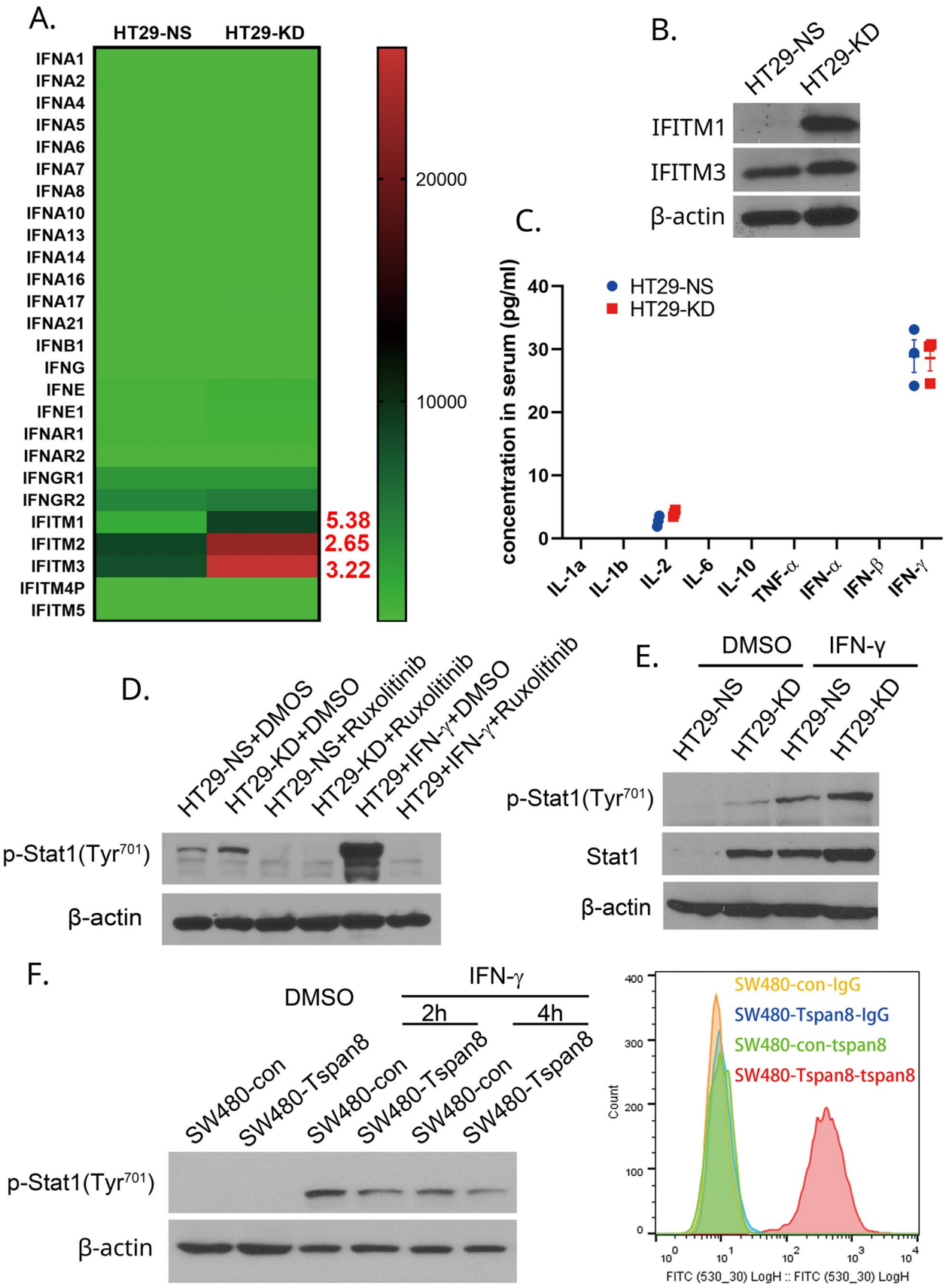
A.
HT29-NS
HT29-KD
IFNA1
IFNA2
IFNA4
IFNA5
IFNA6
IFNA7
IFNA8
IFNA10
IFNA13
IFNA14
IFNA16
IFNA17
IFNA21
IFNB1
IFNG
IFNE
IFNE1
IFNAR1
IFNAR2
IFNGR1
IFNGR2
IFITM1
IFITM2
IFITM3
IFITM4P
IFITM5
5.38
2.65
3.22
20000
10000
B.
HT29-NS
HT29-KD
IFITM1
IFITM3
β-actin
C.
HT29-NS
HT29-KD
concentration in serum (pg/ml)
40
30
20
10
0
IL-1a
IL-1b
IL-2
IL-6
IL-10
TNF-α
IFN-α
IFN-β
IFN-γ
D.
HT29-NS+DMOS
HT29-KD+DMSO
HT29-NS+Ruxolitinib
HT29-KD+Ruxolitinib
HT29+IFN-γ+DMSO
HT29+IFN-γ+Ruxolitinib
p-Stat1(Tyr701)
β-actin
E.
DMSO
IFN-γ
HT29-NS
HT29-KD
HT29-NS
HT29-KD
p-Stat1(Tyr701)
Stat1
β-actin
F.
DMSO
IFN-γ
2h
4h
SW480-con
SW480-Tspan8
SW480-con
SW480-Tspan8
SW480-con
SW480-Tspan8
p-Stat1(Tyr701)
β-actin
SW480-con-IgG
SW480-Tspan8-IgG
SW480-con-tspan8
SW480-Tspan8-tspan8
Count
400
300
200
100
0
FITC (530_30) LogH :: FITC (530_30) LogH

◂**Fig. 3** Tspan8 inhibits IFN-γ-induced activation of Stat1. **A** Heat map showing the expression of the interferon family members, their receptors, and some specific downstream transcriptional products in HT29-NS and HT29-KD cells by cDNA Micro-Array. **B** IFITM1 and IFITM3 proteins were analyzed by Western blot. **C** Measurement of interleukins and interferons in the conditioned media from HT29-NS and HT29-KD transfectant cells was performed with a Human XL Cytokine Luminex Performance Panel Premixed Kit (mean ± SEM, $n=3$ individual samples). **D** Stat1 signaling was analyzed in HT29-NS and HT29-KD cells after the Jak1/2 inhibitor ruxolitinib treatment for 12 h. The HT29 cells treated with IFN-γ and/or ruxolitinib served as controls. **E** With or without exogenous IFN-γ (10 ng/ml) stimulation for 2 h, Stat1 activation was analyzed in HT29-NS and HT29-KD cells by Western blot. **F** With or without exogenous IFN-γ stimulation (10 ng/ml) for 2 h or 4 h, Stat1 signaling was analyzed in SW480-con and SW480-Tspan8 stable transfectant cells by Western blot. The surface levels of Tspan8 on SW480-con and SW480-Tspan8 stable transfectant cells were measured by flow cytometry

IFN-γR1 mainly undergoes clathrin-dependent endocytosis in Tspan8-removed/-absent cells

IFN-γR1 can be internalized through clathrin- and lipid raft-dependent endocytosis pathways [45]. To determine how Tspan8 regulates IFN-γR1 endocytosis, we used Dynasore, a dynamin inhibitor, to inhibit clathrin-dependent endocytosis and Filipin, a cholesterol sequester, to inhibit lipid raft-dependent endocytosis. For HT29 cells, Dynasore shifted the vesicle-type staining of IFN-γR1 from a perinuclear distribution pattern to a peripheral distribution pattern in the aggregate of multiple cells (Fig. 5A, top panel). Filipin exerts similar but even more obvious effect (Fig. 5A, top panel). These changes suggest that both endocytic pathways contribute to IFN-γR1 endocytosis in HT29 cells. Upon Dynasore treatment, almost no puncta or vesicle-like staining of IFN-γR1 was observed in HT29-KD cells in immunofluorescence (Fig. 5A, bottom panel). Filipin treatment also diminished the puncta or vesicle-like staining of IFN-γR1 in HT29-KD cells, but to less extend than Dynasore treatment (Fig. 5A, bottom panel).

Both Dynasore and Filipin elevated the cell surface level of IFN-γR1 in HT29 cells, revealed by flow cytometry analysis (Fig. 5B, left panel), likely by inhibiting IFN-γR1 endocytosis, supporting the notion that both endocytic pathways contribute to IFN-γR1 endocytosis in HT29 cells. IFN-γR1 at the surface of HT29-KD cells treated with Dynasore returned to the same level as that of HT29-NS cells, and IFN-γR1 at the surface of HT29-KD cells treated with Filipin also became increased, with partial rescue (Fig. 5B, right panel).

Caveolae are invaginated lipid rafts and also undergo dynamin-dependent endocytosis. Earlier electron microscopy studies found that IFN-γ and IFN-γR1 are colocalized in the caveolin (CAV)-containing structures and clathrin-coated pits in human lymphoma cells [48]. However, cavin-1, which is required for caveola formation [49], was not expressed in HT29-NS and HT29-KD cells (Fig. S5A), although CAV-1 and CAV-2 were very much decreased upon Tspan8 knockdown. Therefore, we predict that caveolae do not exist in HT29 cells. Furthermore, immunofluorescence indicated that IFN-γR1 was not colocalized with CAV-1 in either HT29-NS or HT29-KD cells (Fig. S5B). Hence, caveolae were excluded from Tspan8-regulated endocytosis of IFN-γR1.

Dynasore also made p-Stat1 (Tyr^{701}) and its transcriptional product IFITM1 undetectable in HT29-KD cells (Fig. 5C), and total cellular level of IFN-γR1 was reduced by Dynasore to the level in HT29-NS cells. However, after Filipin treatment, p-Stat1 (Tyr^{701}) and IFITM1 were decreased in HT29-KD cells but IFN-γR1 remained no change (Fig. 5C). SW480 cells, which have almost no Tspan8 expression as aforementioned, were treated with DMSO, Dynasore, or filipin for 6 h, followed by IFN-γ stimulation for 30 min. In the Dynasore-treated SW480 cells IFN-γ-induced activation of Stat1 was almost lost, while filipin did not alter IFN-γ-induced activation of Stat1 (Fig. 5D), indicating that dynamin-dependent endocytosis is needed for Stat1 activation.

Taking together, Tspan8 prevents IFN-γR1 from undergoing clathrin-dependent endocytosis, and clathrin-coated pits determine IFN-γR1 endocytosis and subsequent Stat1 activation in Tspan8-silenced or -absent cells.

Tspan8 is partially localized in lipid rafts and links IFN-γR1 to lipid rafts

Endocytosis of IFN-γR1 is usually mediated by lipid rafts [47], which are enriched in cholesterol and sphingolipids, such as ganglioside GM1. The clathrin-dependent endocytosis of IFN-γR1 in HT29 cells upon Tspan8 silencing drives us to explore the relationship between Tspan8 and lipid rafts. In HT29 cells, Tspan8 and GM1 were largely colocalized together by confocal microscopy, with Mander's correlation coefficient M1 more than 0.5 and M2 up to 0.7 (Fig. 6A), suggesting that Tspan8 is mainly present in GM1-containing lipid rafts. In addition, a line-scan analysis revealed extensive overlap between Tspan8 and GM1 signals (Fig. 6A). Tspan8 and GM1 were also colocalized in SW480-Tspan8 cells, and the colocalizations were largely distributed at the cell–cell contact (Fig. 6B). Using super-resolution imaging SIM, we found that Tspan8 proteins were colocalized with GM1 molecules at the planar region plasma membrane, at the basal region or neck of GM1-enriched plasma membrane blebs, and in cytoplasmic area (Fig. 6C, enlarged insets on upper right, lower right, and left, respectively). Tspan8 could colocalize with GM1 at the cell surface or cell periphery, but the majority of Tspan8 appeared to be distributed in the submembranous region in contrast to the superficial distribution of GM1 (Fig. 6C, enlarged inset on lower right).

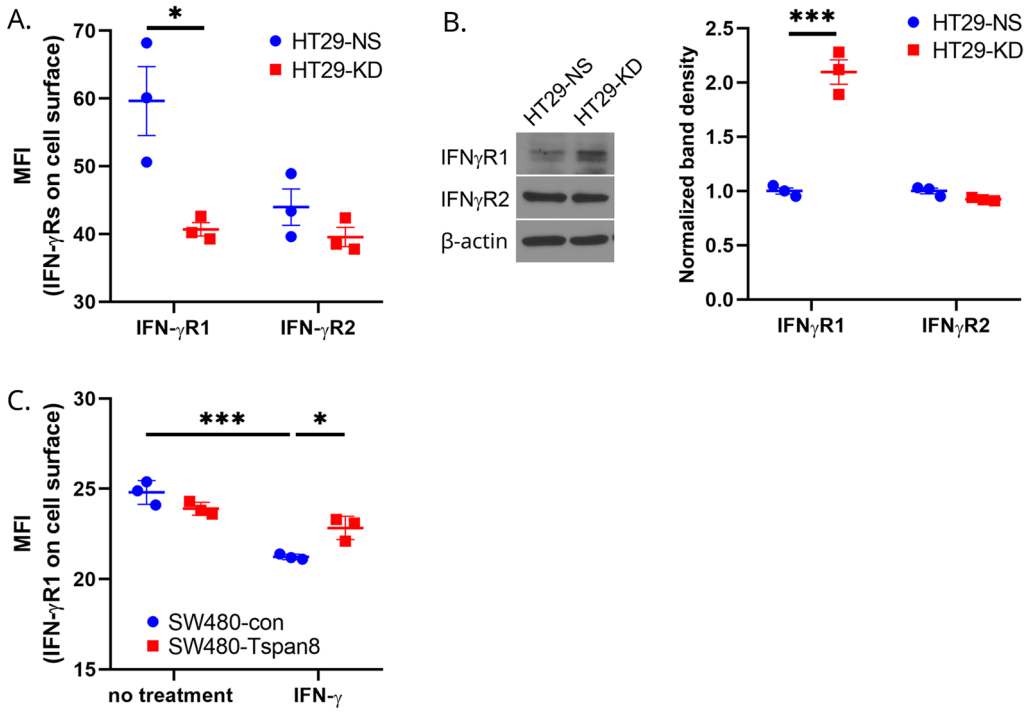

Fig. 4 Tspan8 regulates IFN-γR1 endocytosis upon IFN-γ stimulation. **A** IFN-γR1 and IFN-γR2 on the cell surface were analyzed by flow cytometry, and their levels are presented as MFI (mean ± SEM, $n = 3$ individual experiments). *$p < 0.05$. **B** Total cellular levels of IFNγR1 and IFNγR2 were analyzed by Western blot, and quantification analysis was performed (mean ± SEM, $n = 3$ individual experiments). ***$p < 0.001$. **C** IFNγR1 in the plasma membrane was detected by flow cytometry in SW480-con and SW480-tspan8 cells, with and without IFNγ (10 ng/ml for 5 min) treatment, and their levels are presented as MFI (mean ± SEM, $n = 3$ individual experiments). *$p < 0.05$ and ***$p < 0.001$

The cell surface level of GM1 decreased but total cellular level of GM1 remained unchanged in HT29-KD cells, compared to HT29-NS. In contrast, the GM1 level at the cell surface of SW480-Tspan8 cells was upregulated and total cellular level of GM1 was unchanged, compared to those of SW480-con cells (Fig. 6D). Hence, Tspan8 appears to coalesce with GM1-containing lipid rafts and sustain their presence at the cell surface. For other markers of or related to lipid rafts, flotilin-1 and stomatin remained comparable in HT29 cells between the two groups (Fig. S5A). As no cavin exists in HT29 cells, CAV-1 and CAV-2 proteins were likely present in non-caveolar lipid rafts and became significantly decreased upon Tspan8 silencing (Fig. S5A).

Likewise, Tspan8 and IFN-γR1 were also colocalized with each other in HT29 cells, with M1 and M2 coefficients approximately 0.5 (Fig. 6E). The Tspan8-IFN-γR1 colocalization was also obvious in SW480-Tspan8 transfectant cells and mainly occurred in intracellular vesicle-type structure (Fig. 6F). IFN-γ stimulation did not significantly alter the colocalization in both SW480-Tspan8 cells (Fig. 6F) and HT29 cells (Fig. S6A). Using super-resolution imaging SIM, we found that Tspan8 was colocalized with IFN-γR1 in intracellular vesicles (Fig. 6G, enlarged insets), presumably endosomes. Hence, Tspan8 interacts with IFN-γR1 not only functionally but also probably physically, to keep IFN-γR1 in lipid rafts at the plasma membrane for lipid raft-dependent endocytosis. To explore their putative physical interactions, we performed co-immunoprecipitation and found Tspan8 and IFN-γR1 did not co-immunoprecipitate in HT29 cells under the 1% Brij98 cell lysis condition (Fig. S6B). Using proximity ligation assay (PLA), we also found no positive signals between Tspan8 and IFN-γR1 in IFN-γ stimulated HT29 cells, while positive signals exist between Tspan8 and IFN-γR1 (Fig. S6C), as expected. Without IFN-γ stimulation, no PLA signal exists between Tspan8 and IFN-γR1 either (data not shown). Thus, Tspan8 and IFN-γR1 do not display detectable physical interaction in HT29 cells.

Tspan8 removal alters the IFNγR1 endocytosis route: from lipid raft-dependent to clathrin-dependent endocytosis

Now that Tspan8 supports IFN-γR1 presence in lipid rafts, we investigated the effect of Tspan8 on the distribution of

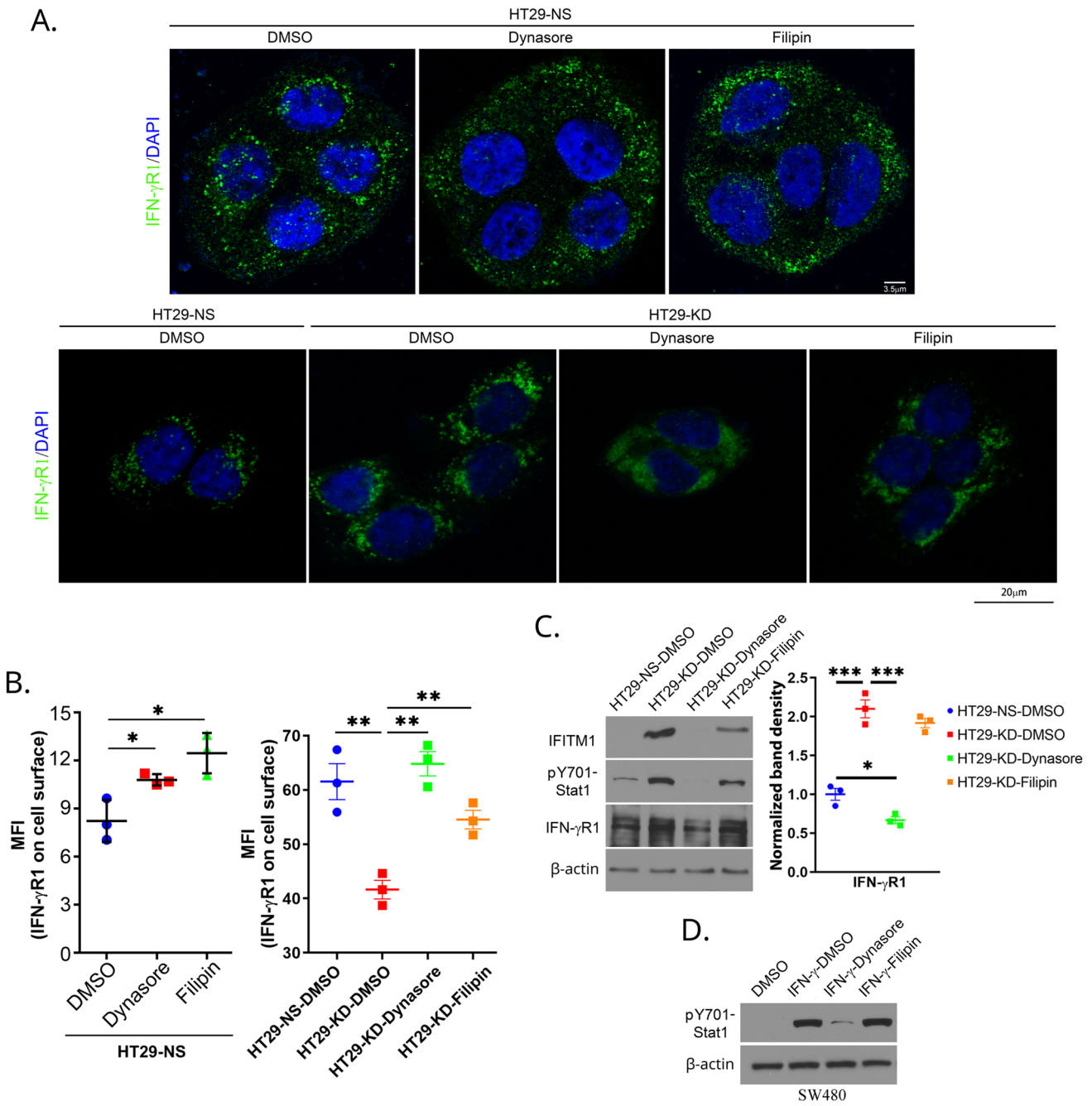

Fig. 5 IFN-γ-induced IFN-γR1 endocytosis and stat1 activation in the absence of Tspan8 depend mainly on clathrin, not lipid rafts. **A** Immunofluorescence of IFN-γR1 in HT29-NS and HT29-KD cells after treatments with DMSO, Dynasore (100 μM), and Filipin (5 μg/ml) for 6 h. IFN-γR1 (green) and DAPI (blue). **B** Flow cytometry was performed to measure the levels of IFN-γR1 on the cell surface after treatments with DMSO, Dynasore (100 μM), and Filipin (5 μg/ml) for 6 h. IFN-γR1 levels are presented as MFI (mean ± SEM, $n = 3$ individual experiments). *$p < 0.05$ and **$p < 0.01$. **C** Western blots for IFITM1, p-Stat1 (Tyr^{701}), and IFN-γR1 were performed after treatment with DMSO, Dynasore, and Filipin for 6 h. Quantitative analysis on IFN-γR1 was shown (mean ± SEM, $n = 3$ individual experiments). *$p < 0.05$ and ***$p < 0.001$. **D** p-Stat1 (Tyr^{701}) was analyzed by Western blot in SW480 cell with DMSO, Dynasore (100 μM), and Filipin (5 μg/ml) treatment for 6 h, followed by IFN-γ stimulation for 30 min

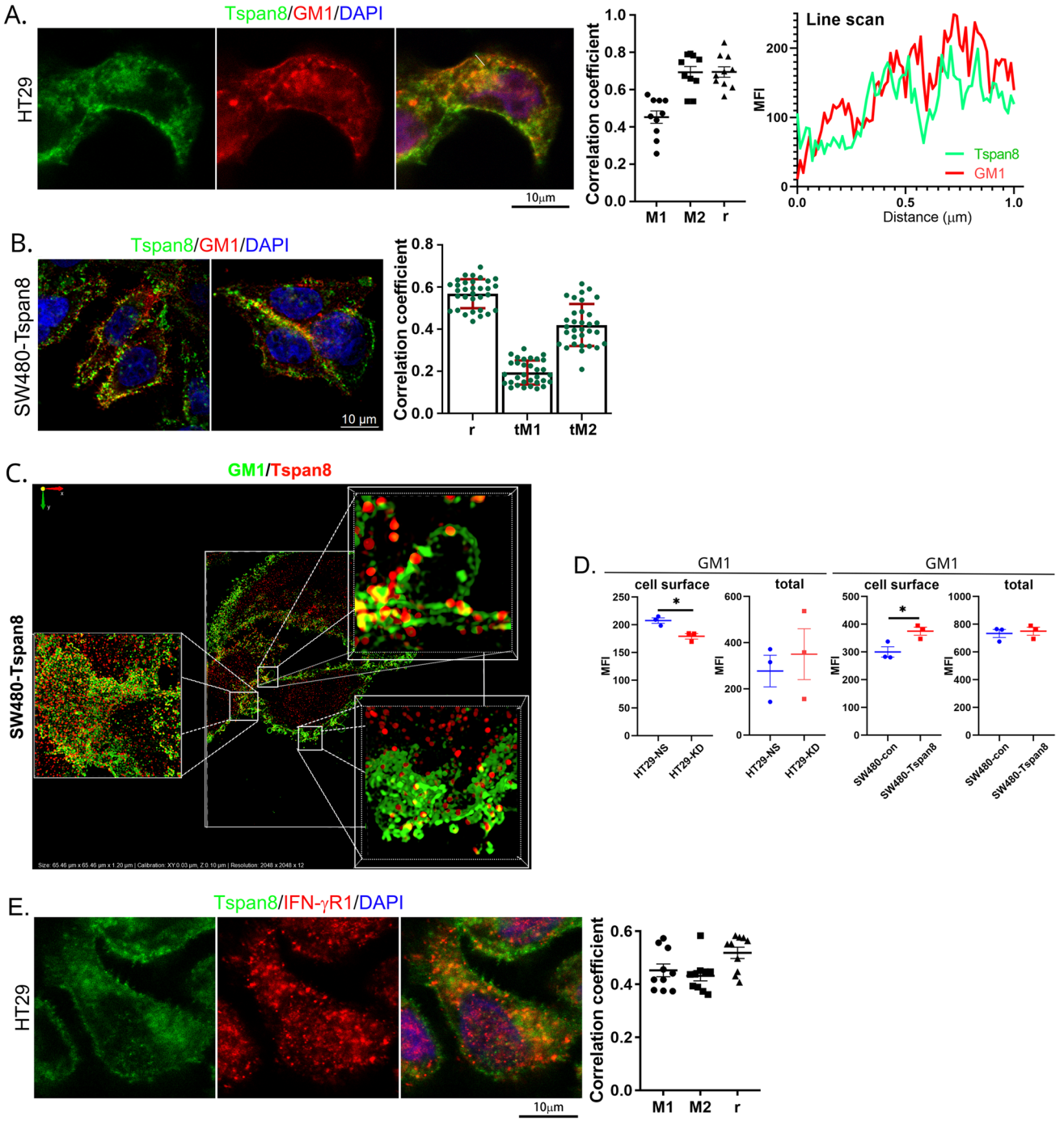

Fig. 6 Tspan8 partitions in lipid rafts and colocalizes with IFN-γR1 in colorectal cancer cells. **A**, **B** Immunofluorescence analysis of GM1 and Tspan8 in HT29 cells (**A**) and SW480-Tspan8 cells (**B**): GM1 (AlexaFluor-594, red) and Tspan8 (AlexaFluor-488, green). Their colocalizations were examined with Mander's and Pearson correlation coefficients (mean ± SEM, $n = 10–32$ cells) and with line scan analysis. **C** SIM analysis on the distributions of GM1 and Tspan8 in SW480-Tspan8 cells. The cells were fixed with 4% paraformaldehyde for 10 min, without permeabilization. A representative z-slice of z-stack (0.1 μm increment) series of a cell was selected for global view of the cell, and the insets present enlarged 3D volume view or 3D-rendered multiple section of z-stack. **D** Flow cytometry analyses on the cell surface and total cellular levels of GM1 in HT29-NS and HT29-KD cells and in SW480-con and SW480-Tspan8 cells (mean ± SEM, $n = 3$ individual experiments). **E**, **F** Immunofluorescence analysis on the distribution of Tspan8 and IFN-γR1 in HT29 cells (**E**) and SW480-Tspan8 cells (**F**). The cells were fixed with 4% paraformaldehyde for 10 min and permeabilized with 0.1% Triton-X100 for 40 s. Tspan8 and IFN-γR1 colocalizations were presented as Mander's and Pearson correlation coefficients (mean ± SEM, $n = 10–35$ cells). For IFN stimulation, the cells were treated with IFN-γ (0.05 ng/ml) for 30 min. **G** SIM analysis on the distribution of IFN-γR1 and Tspan8 in SW480-Tspan8 cells. Insets are shown for enlarged, 3D-rendered or 3D volume view of vesicular staining

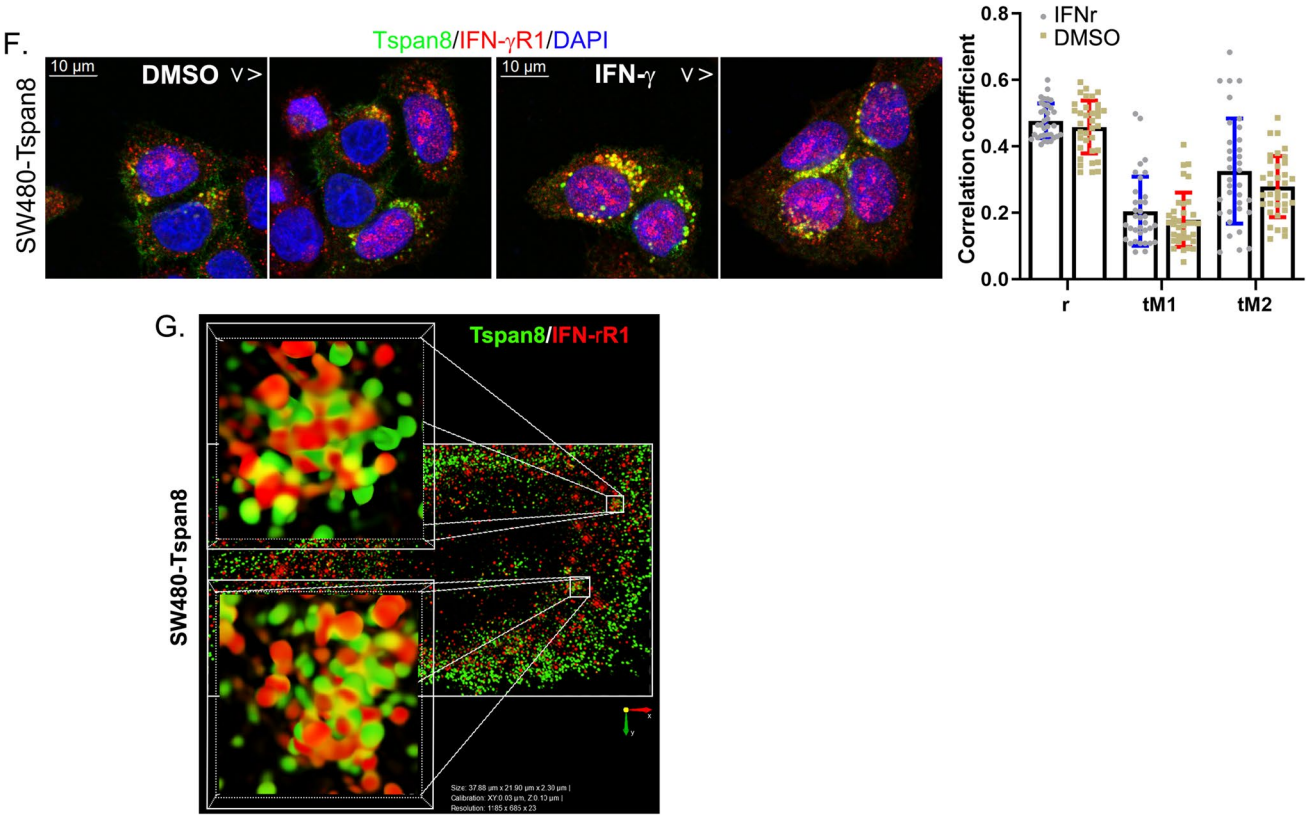

Fig. 6 (continued)

IFN-γR1 in the plasma membrane. By immunofluorescence, we found that in HT29-NS cells IFN-γR1 displayed substantial colocalization with CD44, which typically locates in and internalizes via lipid rafts, with Mander's correlation coefficients M1 and M2 as 0.4 and 0.7, respectively (Fig. 7A). Upon Tspan8 silencing, the co-localization of CD44 with IFN-γR1 was markedly reduced, with Mander's correlation co-efficient M1 down to 0.2 (Fig. 7A), despite of fewer CD44 and IFN-γR1 present at the cell surface upon Tspan8 silencing (Fig. 5B) [23].

In contrast, the co-localization of IFN-γR1 with clathrin notably increased in HT29-KD cells, with impressive elevation in M2 coefficient, compared to HT29-NS (Fig. 7B). Meanwhile, the expression of clathrin protein also decreased in HT29-KD cells (Fig. 7C). These observations further support the notion that Tspan8 knockdown switches IFN-γR1 endocytosis from lipid raft-mediate pathway to clathrin-dependent mechanism. Moreover, in TEER assay, we treated HT29-NS monolayers with IFN-γ and HT29-KD monolayers with Dynasore and found that exogenous IFN-γ disrupted the barrier function and escalated the permeability of HT29-NS monolayers, while Dynasore ultimately restored the barrier function and gradually diminished the permeability of HT29-KD monolayers (Fig. 7D). The observation demonstrates that Tspan8 restrains a clathrin-dependent internalization of IFN-γR1 and subsequent activation of Stat1, to stabilize intestinal epithelial barrier and prevent inflammation.

Discussion

Tspan8 sustains intestinal epithelial barrier function, restrains epithelial paracellular permeability, and is associated with intestine inflammation

Intestinal epithelium is characterized by a polarized arrangement of epithelial cells, and normal intestinal function is based on the sound epithelial barrier. In the present study, we found that Tspan8 is expressed in polarized intestinal cells, and exhibits significant positive correlations with CLDN2, CLDN3, CLDN4, and CDH1, and supports the epithelial barrier function. Increased paracellular permeability upon Tspan8 silencing was observed in epithelial barrier models in vitro. Earlier studies on Tspan8 were mainly focused on cancer. However, our analysis based on GEO database reveals that Tspan8 expression is downregulated in ulcerative colitis model, whose epithelial barrier is notably undermined by inflammation,

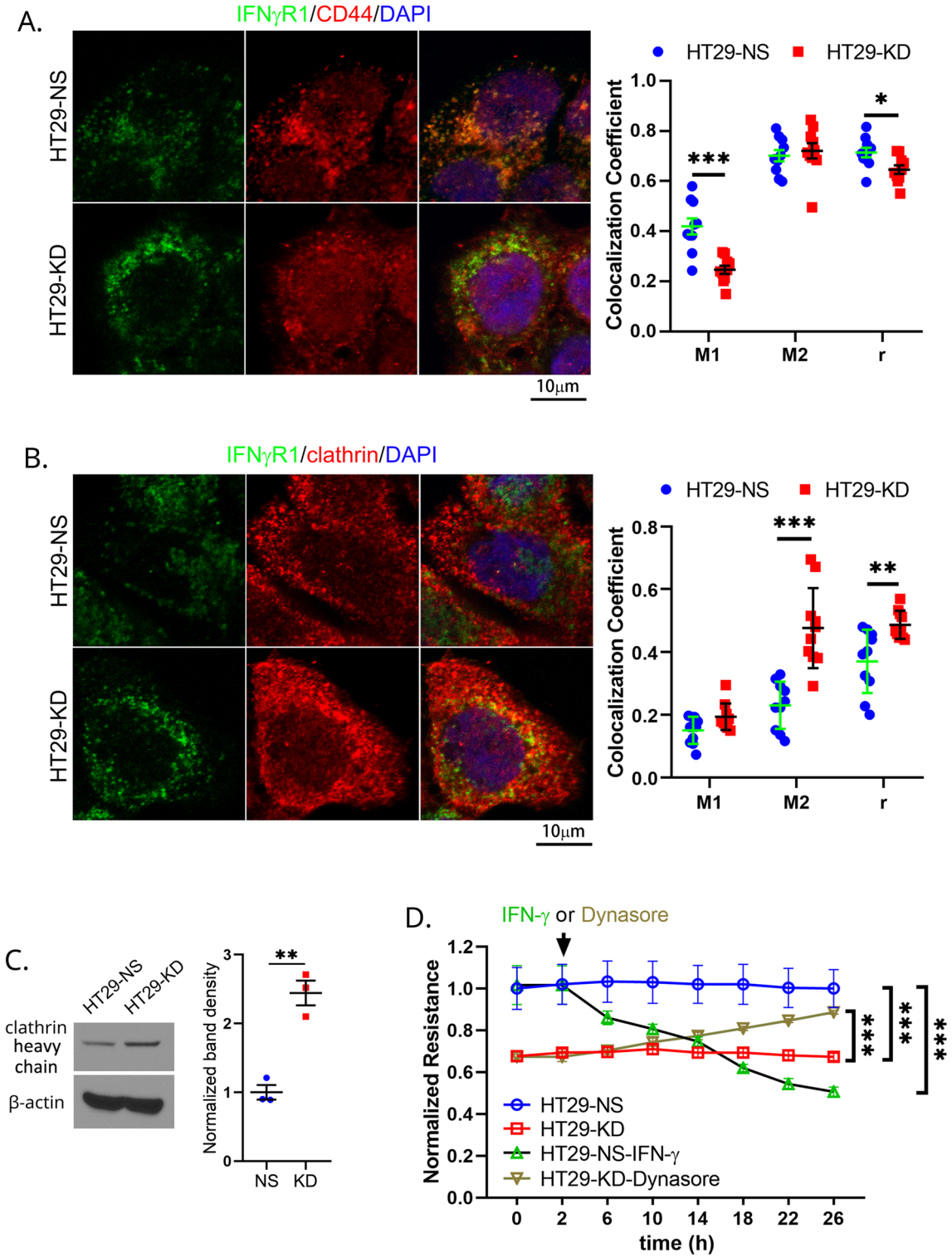

Fig. 7 Tspan8 alters the distribution of IFN-γR1 in plasma membrane. **A** Colocalization of IFN-γR1 and CD44 in HT29-NS and HT29-KD was analyzed by immunofluorescence. Mander's and Pearson's correlation coefficients were performed for the levels of their colocalization (mean ± SEM, $n = 10$ cells). $^{*}p < 0.05$ and $^{***}p < 0.001$. **B** Colocalization of IFN-γR1 and clathrin in HT29-NS and HT29-KD was analyzed by immunofluorescence. Mander's and Pearson's correlation coefficients were performed for the levels of their colocalization (mean ± SEM, $n = 10$ cells). $^{**}p < 0.01$ and $^{***}p < 0.001$. **C** Protein levels of clathrin heavy chain in HT29-NS and HT29-KD cells were examined by Western blot, and quantitative analysis on the band density was performed (mean ± SEM, $n = 3$ individual experiments). $^{**}p < 0.01$. **D** Changes in relative electric resistance were analyzed with the HT29-NS and HT29-KD monolayers that were treated with or without IFN-γ or Dynasore (mean ± SEM, $n = 12$ wells). $^{***}p < 0.001$

underlining the putative importance of Tspan8 in intestine inflammatory disease.

Tspan8 determines IFN-γR1 endocytosis and turnover to inhibit interferon-Stat1 signaling

IFNs-initiated Stat1 signaling is typically activated in virus infection, but also involved in intestinal inflammation. IFNs-induced Stat1 signaling is often considered as a signature in IBD patients and animal models [50–52]. Interestingly, in our study Tspan8 knockdown enhances Stat1 signaling, which is dependent on IFN-γ, not IFN-α/β. Instead of increasing IFN-γ expression, Tspan8 changes the endocytosis of IFN-γR1, but does not affect IFN-γR2. Furthermore, silencing of Tspan8 leads to more accumulation of IFN-γR1 clusters in cytoplasm and then prolonged Stat1 signaling. Thus, Tspan8 downregulation creates a feed forward loop for persistent IFN-γ-induced Stat1 signal activation.

Tspan8 coalescence to lipid rafts promotes IFN signaling turnover

As (i) cholesterol-binding motifs (CBMs) are identified in 30 out of 33 human tetraspanins [53] and (ii) cholesterol binding of tetraspanins CD81, CD9, and CD53 are showed by crystallography [54], interaction with cholesterol could be a general property for many if not all tetraspanins and also suggests physical crosstalk between TEMs and lipid rafts. Tetraspanins such as CD9, CD81, and CD82 were reported to coalesce to lipid rafts to modulate transmembrane signaling [55–57]. In fact, colocalization of Tspan8 with GM1, a marker of lipid rafts, found in this study strengthens this notion. Tspan8 knockdown or overexpression decreases or increases on the cell surface distribution of GM1, respectively, indicating that Tspan8 is not only a resident of but also a modulator for lipid rafts. Importantly, Tspan8 restricts IFN-γR1 in the proximity of lipid rafts and makes IFN-γR1 internalized by lipid rafts, to quench off IFN-γ-initiated signaling.

Tspan8 switches IFN-γR1 from clathrin-dependent to lipid raft-dependent endocytosis route, to limit Stat1 activation magnitude and duration

In human and mouse IFN-γR1, a motif [V-XX-TL-XX-IY] in the transmembrane domain was identified to mediate direct interaction with sphingolipids after IFN-γ binding [58]. Meanwhile, a cholesterol-binding motif [(L/V)-X1–5-Y-X1–5-(R/K)] was also found in the transmembrane domain of IFN-γR1, while glycosylation appears to be important for IFN-γR2 partition to lipid rafts for stat1 activation [59]. In addition, in the patients infected by the intercellular parasite Leishmania donovani, which decreases cholesterol in the plasma membrane, IFN-γ failed to induce IFN-γR1 localization into lipid rafts and activate stat1 signaling [60]. These findings imply an important role of lipid raft in IFN-γR1 clustering and subsequently Jak-Stat1 signaling activation.

While IFN-γR1 is internalized through both clathrin-dependent route and lipid raft-mediated pathway, however, downstream activated Stat1 signaling cannot be blocked by inhibition of clathrin-dependent machinery, but can be blocked by cholesterol sequester [45, 47]. Hence, it was thought that Stat1 is likely to first be recruited to IFN-γR1-abundant lipid raft and be phosphorylated at the plasma membrane, prior to the internalization of IFN-γR1 complex by clathrin-dependent endocytosis [61]. In our study, when Tspan8 was silenced, the elevated Stat1 signaling can be almost fully abrogated by Dynasore, while increases in IFN-γR1 endocytosis and Stat1 activation were only rescued partially by Filipin. When Tspan8 is overexpressed, inhibition of clathrin-dependent machinery almost abolishes IFN-γ-induced Stat1 signaling, but wrecked lipid raft by sequestering cholesterol has no effect on Stat1 signaling. The results imply that loss of Tspan8 prevents Stat1 signaling activation through lipid rafts, but promote a clathrin- and dynamin-dependent pattern. Furthermore, Tspan8 silencing directly induces less localization of IFN-γR1 in or near lipid raft but more localization with clathrin. This finding further supports a critical role of Tspan8 in lipid raft in control of IFN-γR1 endocytosis and Stat1 signaling.

In conclusion, our findings reveal that Tspan8 prevents IFN-γR1 from endocytosis through clathrin pathway by maintaining IFN-γR1 in lipid rafts. Upon Tspan8 loss or reduction, IFN-γ-induced IFN-γR1 endocytosis mainly goes through clathrin-dependent route to promote or prolong Stat1 signaling. Therefore, Tspan8 stabilizes epithelium by preventing overt or long-lasting activation of pro-inflammatory signaling.

Supplementary Information The online version contains supplementary material available at https://doi.org/10.1007/s00018-023-04803-x.

Acknowledgements We thank Dr. Claude Boucheix for special reagents and Ms. Kathy Kyler for English editing. We acknowledge the functional genomics core of Stephenson Cancer Center at the University of Oklahoma Health Sciences Center for technical support. The Nikon N-SIM-E/STORM super-resolution microscope is supported by a Large Equipment Grant from the Oklahoma Center for Adult Stem Cell Research (OCASCR) and the OUHSC Department of Cell Biology.

Author contributions JM designed and performed most experiments, analyzed the data, and wrote the manuscript. SY, YC, DV, SLi, JDW. SLiu, and CJ contributed bio-informatics and statistics analyses. SY, YC SLi, JW, YD, JC, and ZW performed experiments. BL, AC, ZU and

TK provided technical setup and expertise. CG made Tspan8 monoclonal antibodies. JP supervised the proteomic study. XAZ conceived the study, designed experimental approaches, supervised the study, and wrote the manuscript.

Funding This work was supported by National Institutes of Health grants HL137819, GM135547, and AG068581, OCAST grant HR20-055, and research grants from OCASCR, a program of TSET, to XAZ. XAZ is an Oklahoma TSET Cancer Research Scholar.

Data availability All data are available in the main text or the supplementary materials.

Declarations

Conflict of interest The authors declare no competing interests.

References

1. Odenwald MA, Turner JR (2017) The intestinal epithelial barrier: a therapeutic target? Nat Rev Gastroenterol Hepatol 14:9–21. https://doi.org/10.1038/nrgastro.2016.169
2. Katz KD, Hollander D, Vadheim CM et al (1989) Intestinal permeability in patients with Crohn's disease and their healthy relatives. Gastroenterology 97:927–931. https://doi.org/10.1016/0016-5085(89)91499-6
3. Smalley-Freed WG, Efimov A, Burnett PE et al (2010) p120-catenin is essential for maintenance of barrier function and intestinal homeostasis in mice. J Clin Investig 120:1824–1835. https://doi.org/10.1172/JCI41414
4. Suzuki T (2013) Regulation of intestinal epithelial permeability by tight junctions. Cell Mol Life Sci 70:631–659. https://doi.org/10.1007/s00018-012-1070-x
5. Casellas F, Aguade S, Molero J (1986) Intestinal permeability in inflammatory bowel disease. Am J Gastroenterol 81:502
6. Schnoor M (2015) E-cadherin is important for the maintenance of intestinal epithelial homeostasis under basal and inflammatory conditions. Dig Dis Sci 60:816–818. https://doi.org/10.1007/s10620-015-3622-z
7. Luissint AC, Parkos CA, Nusrat A (2016) Inflammation and the intestinal barrier: leukocyte–epithelial cell interactions, cell junction remodeling, and mucosal repair. Gastroenterology 151:616–632. https://doi.org/10.1053/j.gastro.2016.07.008
8. Ahmad R, Sorrell MF, Batra SK, Dhawan P, Singh AB (2017) Gut permeability and mucosal inflammation: bad, good or context dependent. Mucosal Immunol 10:307–317. https://doi.org/10.1038/mi.2016.128
9. Meddings J (2008) What role does intestinal permeability have in IBD pathogenesis? Inflamm Bowel Dis 14(Suppl 2):S138–S139. https://doi.org/10.1002/ibd.20719
10. Hemler ME (2005) Tetraspanin functions and associated microdomains. Nat Rev Mol Cell Biol 6:801–811. https://doi.org/10.1038/nrm1736
11. Charrin S, Jouannet S, Boucheix C, Rubinstein E (2014) Tetraspanins at a glance. J Cell Sci 127:3641–3648. https://doi.org/10.1242/jcs.154906
12. Pan SJ, Wu YB, Cai S et al (2015) Over-expression of tetraspanin 8 in malignant glioma regulates tumor cell progression. Biochem Biophys Res Commun 458:476–482. https://doi.org/10.1016/j.bbrc.2015.01.128
13. El Kharbili M, Agaesse G, Barbollat-Boutrand L et al (2019) Tspan8-beta-catenin positive feedback loop promotes melanoma invasion. Oncogene 38:3781–3793. https://doi.org/10.1038/s41388-019-0691-z
14. Gesierich S, Paret C, Hildebrand D et al (2005) Colocalization of the tetraspanins, CO-029 and CD151, with integrins in human pancreatic adenocarcinoma: impact on cell motility. Clin Cancer Res 11:2840–2852. https://doi.org/10.1158/1078-0432.CCR-04-1935
15. Park CS, Kim TK, Kim HG et al (2016) Therapeutic targeting of tetraspanin8 in epithelial ovarian cancer invasion and metastasis. Oncogene 35:4540–4548. https://doi.org/10.1038/onc.2015.520
16. Greco C, Bralet MP, Ailane N et al (2010) E-cadherin/p120-catenin and tetraspanin Co-029 cooperate for cell motility control in human colon carcinoma. Cancer Res 70:7674–7683. https://doi.org/10.1158/0008-5472.CAN-09-4482
17. Wei L, Li Y, Suo Z (2015) TSPAN8 promotes gastric cancer growth and metastasis via ERK MAPK pathway. Int J Clin Exp Med 8:8599–8607
18. Zhu R, Gires O, Zhu L et al (2019) TSPAN8 promotes cancer cell stemness via activation of sonic Hedgehog signaling. Nat Commun 10:2863. https://doi.org/10.1038/s41467-019-10739-3
19. Wang H, Rana S, Giese N, Buchler MW, Zoller M (2013) Tspan8, CD44v6 and alpha6beta4 are biomarkers of migrating pancreatic cancer-initiating cells. Int J Cancer 133:416–426. https://doi.org/10.1002/ijc.28044
20. Ailane N, Greco C, Zhu Y et al (2014) Effect of an anti-human Co-029/tspan8 mouse monoclonal antibody on tumor growth in a nude mouse model. Front Physiol 5:364. https://doi.org/10.3389/fphys.2014.00364
21. Heo K, Lee S (2020) TSPAN8 as a novel emerging therapeutic target in cancer for monoclonal antibody therapy. Biomolecules. https://doi.org/10.3390/biom10030388
22. Schafer D, Tomiuk S, Kuster LN et al (2021) Identification of CD318, TSPAN8 and CD66c as target candidates for CAR T cell based immunotherapy of pancreatic adenocarcinoma. Nat Commun 12:1453. https://doi.org/10.1038/s41467-021-21774-4
23. Guo Q, Xia B, Zhang F et al (2012) Tetraspanin CO-029 inhibits colorectal cancer cell movement by deregulating cell–matrix and cell–cell adhesions. PLoS One 7:e38464. https://doi.org/10.1371/journal.pone.0038464
24. Sirven A, Ravet E, Charneau P et al (2001) Enhanced transgene expression in cord blood CD34(+)-derived hematopoietic cells, including developing T cells and NOD/SCID mouse repopulating cells, following transduction with modified trip lentiviral vectors. Mol Ther 3:438–448. https://doi.org/10.1006/mthe.2001.0282
25. Franken NA, Rodermond HM, Stap J, Haveman J, van Bree C (2006) Clonogenic assay of cells in vitro. Nat Protoc 1:2315–2319. https://doi.org/10.1038/nprot.2006.339
26. Zweibaum A, Pinto M, Chevalier G et al (1985) Enterocytic differentiation of a subpopulation of the human colon tumor cell line HT-29 selected for growth in sugar-free medium and its inhibition by glucose. J Cell Physiol 122:21–29. https://doi.org/10.1002/jcp.1041220105
27. Le Bivic A, Hirn M, Reggio H (1988) HT-29 cells are an in vitro model for the generation of cell polarity in epithelia during embryonic differentiation. Proc Natl Acad Sci USA 85:136–140. https://doi.org/10.1073/pnas.85.1.136

28. Matter K, Balda MS (2003) Functional analysis of tight junctions. Methods 30:228–234. https://doi.org/10.1016/s1046-2023(03)00029-x
29. Bai B, Tan H, Pagala VR et al (2017) Deep profiling of proteome and phosphoproteome by isobaric labeling, extensive liquid chromatography, and mass spectrometry. Methods Enzymol 585:377–395. https://doi.org/10.1016/bs.mie.2016.10.007
30. Wang Z, Yu K, Tan H et al (2020) 27-Plex tandem mass tag mass spectrometry for profiling brain proteome in Alzheimer's disease. Anal Chem 92:7162–7170. https://doi.org/10.1021/acs.analchem.0c00655
31. Wang H, Yang Y, Li Y et al (2015) Systematic optimization of long gradient chromatography mass spectrometry for deep analysis of brain proteome. J Proteome Res 14:829–838. https://doi.org/10.1021/pr500882h
32. Bai B, Wang X, Li Y et al (2020) Deep multilayer brain proteomics identifies molecular networks in Alzheimer's disease progression. Neuron 106:700. https://doi.org/10.1016/j.neuron.2020.04.031
33. Wang X, Li Y, Wu Z, Wang H, Tan H, Peng J (2014) JUMP: a tag-based database search tool for peptide identification with high sensitivity and accuracy. Mol Cell Proteom 13:3663–3673. https://doi.org/10.1074/mcp.O114.039586
34. Peng J, Elias JE, Thoreen CC, Licklider LJ, Gygi SP (2003) Evaluation of multidimensional chromatography coupled with tandem mass spectrometry (LC/LC–MS/MS) for large-scale protein analysis: the yeast proteome. J Proteome Res 2:43–50. https://doi.org/10.1021/pr025556v
35. Niu M, Cho JH, Kodali K et al (2017) Extensive peptide fractionation and y1 ion-based interference detection method for enabling accurate quantification by isobaric labeling and mass spectrometry. Anal Chem 89:2956–2963. https://doi.org/10.1021/acs.analchem.6b04415
36. Vanderwall D, Suresh P, Fu Y et al (2021) JUMPn: a streamlined application for protein co-expression clustering and network analysis in proteomics. J Vis Exp. https://doi.org/10.3791/62796
37. Uhlen M, Fagerberg L, Hallstrom BM et al (2015) Proteomics. Tissue-based map of the human proteome. Science 347:1260419. https://doi.org/10.1126/science.1260419
38. Miller HE, Bishop AJR (2021) Correlation AnalyzeR: functional predictions from gene co-expression correlations. BMC Bioinform 22:206. https://doi.org/10.1186/s12859-021-04130-7
39. Asao H, Okuyama C, Kumaki S et al (2001) Cutting edge: the common gamma-chain is an indispensable subunit of the IL-21 receptor complex. J Immunol 167:1–5. https://doi.org/10.4049/jimmunol.167.1.1
40. Subramaniam PS, Torres BA, Johnson HM (2001) So many ligands, so few transcription factors: a new paradigm for signaling through the STAT transcription factors. Cytokine 15:175–187. https://doi.org/10.1006/cyto.2001.0905
41. Sheikh F, Baurin VV, Lewis-Antes A et al (2004) Cutting edge: IL-26 signals through a novel receptor complex composed of IL-20 receptor 1 and IL-10 receptor 2. J Immunol 172:2006–2010. https://doi.org/10.4049/jimmunol.172.4.2006
42. Yoshimoto T, Okada K, Morishima N et al (2004) Induction of IgG2a class switching in B cells by IL-27. J Immunol 173:2479–2485. https://doi.org/10.4049/jimmunol.173.4.2479
43. de Weerd NA, Nguyen T (2012) The interferons and their receptors—distribution and regulation. Immunol Cell Biol 90:483–491. https://doi.org/10.1038/icb.2012.9
44. Forbes LR, Milner J, Haddad E (2016) Signal transducer and activator of transcription 3: a year in review. Curr Opin Hematol 23:23–27. https://doi.org/10.1097/MOH.0000000000000206
45. Marchetti M, Monier MN, Fradagrada A et al (2006) Stat-mediated signaling induced by type I and type II interferons (IFNs) is differentially controlled through lipid microdomain association and clathrin-dependent endocytosis of IFN receptors. Mol Biol Cell 17:2896–2909. https://doi.org/10.1091/mbc.e06-01-0076
46. Chmiest D, Sharma N, Zanin N et al (2016) Spatiotemporal control of interferon-induced JAK/STAT signalling and gene transcription by the retromer complex. Nat Commun 7:13476. https://doi.org/10.1038/ncomms13476
47. Subramaniam PS, Johnson HM (2002) Lipid microdomains are required sites for the selective endocytosis and nuclear translocation of IFN-gamma, its receptor chain IFN-gamma receptor-1, and the phosphorylation and nuclear translocation of STAT1alpha. J Immunol 169:1959–1969. https://doi.org/10.4049/jimmunol.169.4.1959
48. Sadir R, Lambert A, Lortat-Jacob H, Morel G (2001) Caveolae and clathrin-coated vesicles: two possible internalization pathways for IFN-gamma and IFN-gamma receptor. Cytokine 14:19–26. https://doi.org/10.1006/cyto.2000.0854
49. Hill MM, Bastiani M, Luetterforst R et al (2008) PTRF-Cavin, a conserved cytoplasmic protein required for caveola formation and function. Cell 132:113–124. https://doi.org/10.1016/j.cell.2007.11.042
50. McElrath C, Espinosa V, Lin JD et al (2021) Critical role of interferons in gastrointestinal injury repair. Nat Commun 12:2624. https://doi.org/10.1038/s41467-021-22928-0
51. Langer V, Vivi E, Regensburger D et al (2019) IFN-gamma drives inflammatory bowel disease pathogenesis through VE-cadherin-directed vascular barrier disruption. J Clin Investig 129:4691–4707. https://doi.org/10.1172/JCI124884
52. Ghosh S, Chaudhary R, Carpani M, Playford R (2006) Interfering with interferons in inflammatory bowel disease. Gut 55:1071–1073. https://doi.org/10.1136/gut.2005.090134
53. Huang C, Hays FA, Tomasek JJ, Benyajati S, Zhang XA (2020) Tetraspanin CD82 interaction with cholesterol promotes extracellular vesicle-mediated release of ezrin to inhibit tumour cell movement. J Extracell Vesicles 9:1692417. https://doi.org/10.1080/20013078.2019.1692417
54. Zimmerman B, Kelly B, McMillan BJ et al (2016) Crystal structure of a full-length human tetraspanin reveals a cholesterol-binding pocket. Cell 167:1041-1051 e1011. https://doi.org/10.1016/j.cell.2016.09.056
55. Cherukuri A, Shoham T, Sohn HW et al (2004) The tetraspanin CD81 is necessary for partitioning of coligated CD19/CD21-B cell antigen receptor complexes into signaling-active lipid rafts. J Immunol 172:370–380. https://doi.org/10.4049/jimmunol.172.1.370
56. Wei Q, Zhang F, Richardson MM et al (2014) CD82 restrains pathological angiogenesis by altering lipid raft clustering and CD44 trafficking in endothelial cells. Circulation 130:1493–1504. https://doi.org/10.1161/CIRCULATIONAHA.114.011096
57. Zilber MT, Setterblad N, Vasselon T et al (2005) MHC class II/CD38/CD9: a lipid-raft-dependent signaling complex in human monocytes. Blood 106:3074–3081. https://doi.org/10.1182/blood-2004-10-4094
58. Contreras FX, Ernst AM, Haberkant P et al (2012) Molecular recognition of a single sphingolipid species by a protein's

transmembrane domain. Nature 481:525–529. https://doi.org/10.1038/nature10742
59. Blouin CM, Hamon Y, Gonnord P et al (2016) Glycosylation-dependent IFN-gammaR partitioning in lipid and actin nanodomains is critical for JAK activation. Cell 166:920–934. https://doi.org/10.1016/j.cell.2016.07.003
60. Sen S, Roy K, Mukherjee S, Mukhopadhyay R, Roy S (2011) Restoration of IFNgammaR subunit assembly, IFNgamma signaling and parasite clearance in *Leishmania donovani* infected macrophages: role of membrane cholesterol. PLoS Pathog 7:e1002229. https://doi.org/10.1371/journal.ppat.1002229
61. Blouin CM, Lamaze C (2013) Interferon gamma receptor: the beginning of the journey. Front Immunol 4:267. https://doi.org/10.3389/fimmu.2013.00267